Research on Mesoscopic Characteristics of Limestone Grouting Diffusion Based on Discrete Fracture Network

Jiawen Li [1], Shugao Zhan [1], Zuliang Zhong [2], Yi Wang [2, *]

[1] China Construction Tunnel Co., Ltd., Chongqing 401320, China
[2] School of Civil Engineering, Chongqing University, Chongqing 400045, China.

Abstract. The limestone stratum has well-developed rock fissures and abundant groundwater. Under extreme rainstorm conditions, tunnel surrounding rock seepage is serious especially. In order to reveal the grouting diffusion mechanism of karst fractured rock mass and realize effective water plugging, in this paper, the basic mechanical parameters of limestone are obtained by laboratory triaxial test, and the porosity distribution of rock mass is obtained by nuclear magnetic resonance test. The PFC2D discrete element software is used to simulate the mechanical characteristics of compressive deformation and fracture propagation pattern of the limestone and compared with the triaxial test results. Discrete fracture network theory is used to establish PFC2D numerical simulation of grouting diffusion model of fractured rock mass. And the filling diffusion mechanism and stress variation rule of cement slurry in fractured limestone under different grouting pressure are studied. The results show that (1) During the grouting process, the micro-cracks expand along the tip of the existing cracks, and extend to the surrounding cracks to finally form through cracks, so as to achieve the effect of grouting reinforcement. (2) With the increase of grouting pressure, the maximum displacement of particles increases continuously, but with the prolongation of grouting time, the maximum displacement of particles reaches a stable state and no longer increases. (3) During the grouting process of the fractured rock mass, with the increase of grouting time, the stress of the fractured rock mass finally reaches a stable state. This study provides an important reference for the setting of grouting parameters of limestone rock mass.

Keywords: Tunnel engineering, fractured rock mass, PFC2D, limestone, grouting diffusion.

1. Introduction

Subjected to complex geological structure, various structural planes (faults, joints and cracks, etc.) are formed inside the rock mass, which will cut the rock mass into rock blocks of different sizes and shapes, and finally form the fractured rock mass. Due to the complex structure and poor mechanical properties of fractured rock mass, grouting is often used to improve the mechanical properties of fractured rock mass in engineering practice. For the grouting process of fractured rock mass, materials with smaller particle diameter and certain cohesiveness are often used to fill the fractured rock mass with certain pressure. Wang[1] analyzed the strength of fractured rock mass filled by grouting materials based on uniaxial compression test, and the results showed that grouting materials could improve the strength of specimens, delay crack initiation, and reduce the strain at the crack tip. Because the permeability of cracks is much greater than that of pores [2], the grout in the grouting process is mainly spread by cracks, and only a few of them have pore seepage [3]. In actual engineering, the distribution of cracks in rock mass is difficult to identify clearly. So that in engineering construction, empirical design is often used for grouting reinforcement of fractured rock mass, which makes the grouting reinforcement theory of fractured rock mass lag behind the engineering practice.

In recent years, scholars have conducted a large number of grouting tests on fractured rock mass [4-6]. Du[7] discussed the diffusion characteristics of cement slurry in rock under the action of dynamic water through laboratory tests. Ding[8] conducted a grouting diffusion test through a visual test device, and analyzed the spatial-temporal distribution characteristics of the velocity field and pressure field in the process of grouting diffusion, and the results showed that the fracture structure of rock mass had a great influence on the grouting diffusion. Jiang[9] concluded that slurry filling could effectively improve the strength of fractured rock mass through laboratory tests, and analyzed the variation law of grouting pressure, slurry flow and slurry diffusion surface based on three-dimensional grouting test system. Zhang[10] developed a simulation test device for dynamic grouting of fractured rock mass, and determined the law of grouting diffusion

* Corresponding author: Yi Wang

through the grouting test. It can be seen that the grouting test explained the grout diffusion filling process in the crack from the macro aspect, but for the meso aspect, the grout diffusion direction and stress distribution and other problems could not be effectively solved. Based on the rapid development of computer, some scholars used finite element method, finite difference method and discrete element method to build the rock mass grouting model, analyzed the changes of grout velocity field, displacement field and stress field, and further improved the development of grout diffusion filling law. But most of the studies were based on single fissure or orthogonal fissure rock mass [11-13]. There is a certain gap between it and the actual fractured rock mass. In order to objectively describe the grout diffusion and the change law of displacement and stress field of fractured rock mass in the process of grouting, this paper obtained reliable meso-parameters through the comparison and verification of laboratory test and numerical calculation. The random fracture network model in PFC2D was adopted to construct limestone fractured rock mass, and the evolution process of grouting diffusion and deformation law of limestone fractured rock mass are studied. The results are of great significance for the study of grouting parameter setting in limestone fractured rock mass.

2. Project Overview

The Tuzhu tunnel in Chongqing crosses the Guanyin gorge anticline, with small folds, faults, joints and fissures, interlayer sliding scrapes and fracture zones in and around the anticline axis. The underlying bedrock of the tunnel area is mainly Jialingjiang group, partly Leikoupo group, which is hard and mostly fragmented, with joints and fissures between undeveloped and more developed, laminated and generally combined between layers; the stratigraphy is mainly limestone, with occasional muddy rocks, as shown in Figure 1.

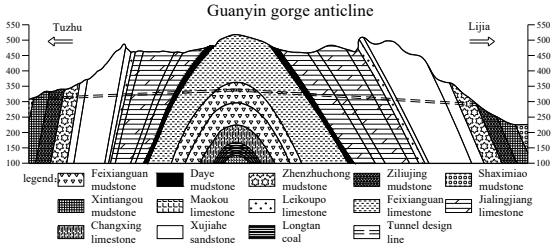

Figure 1: Schematic diagram of the engineering geology of the earth main tunnel

According to the survey, there are more cavities and caves in the soluble rock formations, more tension fissures in the Feixianguan formation in the core of the anticline, and the phenomenon of leakage of groundwater exists in various depth ranges. The presence of fissures and dissolution pores leads to different permeability and water-richness of the rock mass. Engineering disasters such as roof collapse, collapse and large water gushing will occur when the tunnel is driven into the densely fractured section, fault fracture zone and near the boundary of various aquifers, as shown in Figure 2. In the process of tunnel excavation, water leakage from the lining will jeopardize the safety of tunnel construction if it is not blocked in time [14, 15] and cause the surface water level to drop. So the construction process takes targeted grouting and water plugging to achieve the purpose of "mainly blocking and limited discharge" [16], to ensure the safety of tunnel construction and operation, and reduce the impact on the residents' living water.

Figure 2: Tunnel lining water seepage

This paper relies on the curtain grouting treatment section of Chongqing Tuzhu tunnel, as shown in Figure 3. The PFC2D discrete element numerical software is used to simulate the slurry diffusion process based on hydraulic splitting, and the optimal slurry injection pressure and slurry filling diffusion law are obtained by analyzing the evolution of displacement field and stress field during the fractured rock grouting process.

Figure 3: Curtain grouting

3. Parameter Calibration and Model Building

3.1 Parameter Calibration

3.1.1 Particle Mesoscopic Parameter Calibration

The macroscopic properties of rock mass are specifically expressed as the mesoscopic parameters of particles in the particle flow numerical model. After the modeling is

completed, the accuracy of the simulation results largely depends on the precise selection of mesoscopic parameters. Parallel bonding model is adopted between particles. In this test, 12 limestone specimens are selected for calibration of rock mass physical and mechanical parameters, and a total of 6 crack specimens meeting the test requirements are obtained. After the test, 6 samples with obvious macroscopic cracks and good integrity are selected and divided into 2 groups, group A and group B, with 3 samples in each group. In this test, the French TOP INDUSTRLE rock full stress multi-field coupling triaxial tester is used for triaxial test, as shown in Figure 4. The confining pressure is 5 MPa and the vertical loading control is 0.1 mm/min. Numerical software PFC2D is used to simulate limestone specimens with a diameter of 50 mm and a height of 100 mm, as shown in Figure 5.

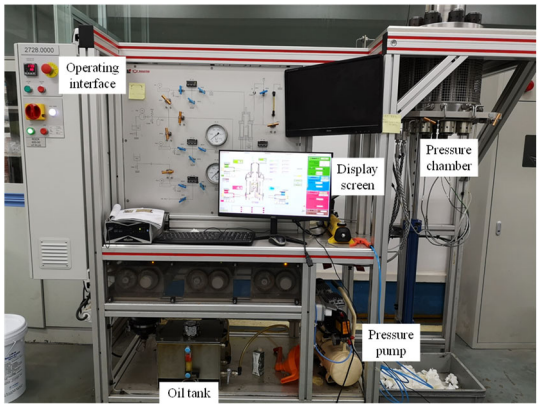

Figure 4: French TOP INDUSTRLE rock total stress multi-field coupling triaxial test instrument

From Figure 5, it can be seen that the limestone is a hard rock, and the average peak strength reaches 185 MPa under the action of the surrounding pressure of 5 MPa. The peak strength of the particle flow simulated limestone specimen matches the test results well and meets the macroscopic consistency. Because this specimen has more internal microcracks, the A2 stress-strain curve exhibits an obvious compression phenomenon in the initial section, then enters the linear elastic phase, and eventually suffers brittle damage due to reaching the peak strength, resulting in a sharp drop in the curve.

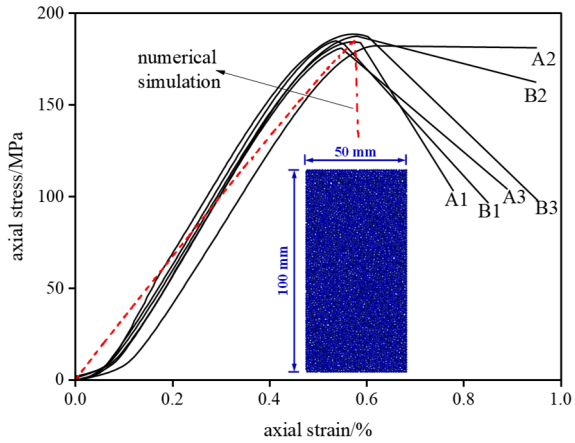

Figure 5: Stress-strain curve of triaxial compression

Under triaxial compression, the fracture morphology of limestone is mainly shear failure (A2, A3, B1, B2, B3), and occasionally V-shaped failure (A1), as shown in Figure 6. By comparing the peak strength and damage morphology of stress-strain curve of the indoor tests and numerical simulations, the granular mesoscopic parameters are determined as shown in Table 1.

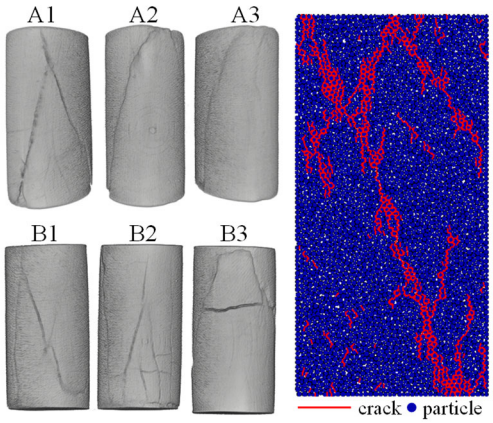

Figure 6: Comparison of failure morphology of limestone specimen between test and numerical simulation

Table 1: Mesoscopic parameters of limestone particles calibrated by triaxial compression test

Granular mesoscopic parameters	Maximum radius (mm)	Minimum radius (mm)	Particle contact modulus (GPa)	Normal tangential stiffness ratio of particles	Particle friction coefficient
	1.5	1	16.6	1.2	0.6
Mesoscopic parameters of parallel bonding	Minimum distance between parallel bonds (mm)	Parallel bonding modulus (GPa)	Parallel bond stiffness ratio	Parallel bond tensile strength (MPa)	Internal cohesion of parallel bond(MPa)
	0.05	16.6	1.2	50	60

3.1.2 *Fluid Mesoscopic Parameters*

Model porosity is a key factor in determining the permeability of cement slurry. The porosity magnitude of intact and fractured rocks are obtained through laboratory tests, so the histogram of porosity distribution of rock distribution is obtained by nuclear magnetic resonance analysis, as shown in Figure 7. The porosity of intact rock ranges from 1.14% to 1.47%, and that of fractured rock ranges from 2.94% to 3.53%. Therefore, to ensure that the numerical simulation is more consistent with the actual situation, the porosity of 3.5% is chosen to simulate the fractured rocks.

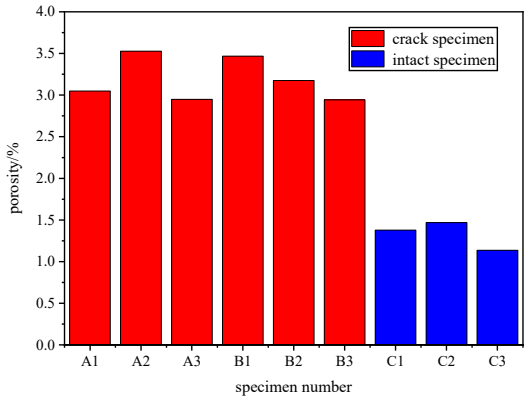

Figure 7: Histogram of porosity distribution

The model permeability coefficient is obtained by reference [17]. Cement slurry is a typical bingham fluid, and the permeability coefficient of water in limestone strata can be obtained by nuclear magnetic resonance. However, it is difficult to obtain the permeability coefficient of cement slurry in limestone strata. The water-cement ratio of cement slurry selected in the test is 1:1. In order to simulate the permeability process of cement slurry in limestone strata, the permeability coefficient of cement slurry in limestone strata can be obtained from formula (1) :

$$k_c = k_0 \frac{\eta_w \rho_c}{\eta_c \rho_w} \quad (1)$$

Where k_c is the permeability coefficient of cement slurry in limestone formation; k_0 is the permeability coefficient of water in limestone; η_w is the dynamic viscosity coefficient of water. η_c is the dynamic viscosity coefficient of cement slurry. ρc is the density of cement slurry; ρ_w is the density of water. The final permeability coefficient of cement slurry in limestone can be determined by the formula (1) as 2.3×10^{-5} cm/s. The mesoscopic parameters of the fluid are finally determined through laboratory test and numerical simulation results, as shown in Table 2:

Table 2: Mesoscopic parameters of fluid

Permeability coefficient(cm/s)	time step	Initial aperture (mm)	Porosity(%)
2.3×10^{-5}	1×10^{-3}	1	3.5

3.2 Modeling of Fractured Rock Mass

In order to describe the distribution of fractures in a rock mass, DFN method is selected, which is to characterize its size, location and occurrence [18]. The fracture distribution function can be obtained from equation (2) :

$$n(l,\theta,\varphi,V) = \alpha(\theta,\varphi) \cdot l^{-r} \cdot V^{\frac{D}{3}} \quad (2)$$

In the formula, l is the fracture length, 35~40 mm; φ is the fracture angle, which is 20~70° in simulation. V is the region where the crack is located, and x and y are -70~70 mm, respectively. r is the scale index of the power law function; n is the power law function of crack distribution; D is the topological dimension (less than 3 in actual calculation). After the generation of fractured rock mass network, although it follows certain mathematical statistics law, the discrete fractured rock network samples can not be accurately expressed. For the crack density calculation method, p10 can accurately calculate the crack frequency value in the sample [19]. Finally, a discrete fracture network model with length and width of 150 mm×150 mm is obtained, as shown in Figure 8. To take into account DFN's conductivity, FISH language is used to break the bond between the particles at the fracture so that the cement slurry fills quickly in the fracture, simulating the realistic characteristics of rapid fissure infusion.

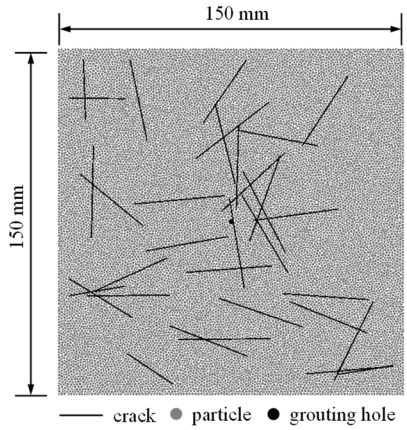

Figure 8: Discrete fracture network model

4. Analysis of Numerical Simulation Results

By using particle flow to simulate the grouting process, the crack propagation and stress distribution of fractured rock mass under the action of grouting pressure can be directly observed, and the grouting process can be better discussed on the mesoscopic level. After the grouting is started, the slurry enters the fluid domain between particles along the pipe from the borehole, as shown in Figure 9. The fluid pressure in the fluid domain and the pipe changes, affecting the contact between particles. As the grouting time progresses, the slurry spreads outwards in a radial pattern. And the energy is consumed in the process of slurry diffusion. When the diffusion reaches a certain distance, the slurry pressure is not sufficient to overcome the resistance within the rock, the slurry stops diffusing and the grouting reinforcement process ends.

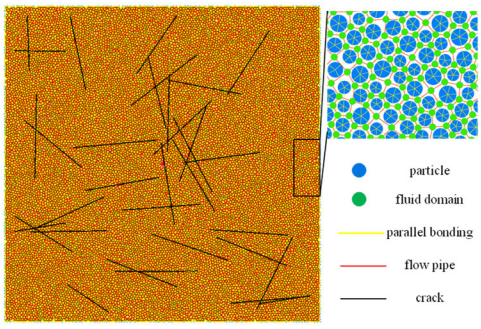

Figure 9: Fluid domain and pipeline model diagram

4.1 Filling and Diffusion Law of Cement Slurry under Different Grouting Pressures

The grout filling diffusion is an important index to test the grouting effect of fractured rock mass. The effects of micro-crack propagation and grout filling under four different grouting pressures at different time steps were simulated numerically. As shown in Figure 10, with the increase of grouting pressure, the number of micro-cracks gradually increases. Under 1 MPa grouting pressure, no new micro-cracks are generated in the fractured rock mass, and only existing cracks are filled. Under 2 MPa grouting pressure, fractured rock mass produces 1 micro-crack. Under the action of 3 MPa and 4 MPa, it produces 8 micro-cracks. However the crack development velocity under 4 MPa grouting pressure is faster than 3 MPa. With the increase of grouting pressure, the crack propagation speed increases gradually, and the first micro-crack is produced under 4 MPa grouting pressure at 2000 time step earlier than 3 MPa and 4000 time step earlier than 2 MPa. It can be seen that with the increase of grouting pressure, the grout diffusion speed is faster and the filling efficiency is higher. Among them, the filling diffusion range under 3 and 4 MPa grouting pressure is consistent and better than 1 and 2 MPa.

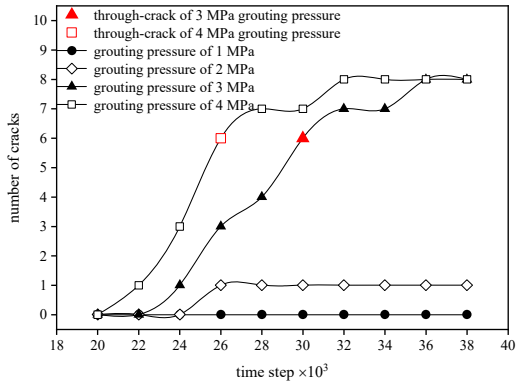

Figure 10: Development of the number of micro-cracks under different grouting pressures

The red micro-cracks in Figure 11 represent the cracks that occur when the grouting pressure exceeds the bonding force between rock particles. The cement slurry is first filled along the existing crack, and then diffuses outward along the grouting hole. Due to the stress concentration at the tip of the existing crack, micro-cracks appear. It can be seen from Figure 11 that the micro-crack develops from the long axis of the existing crack to another crack, and finally forms a through crack. As can be seen from Figure 10, two through cracks formed in the fractured rock mass at the time step of 30,000 and 26000 respectively under the grouting pressure of 3 MPa and 4 MPa, while no through-cracks formed at 2 MPa and 1 MPa. Therefore, crack development can be summarized into three stages: the first stage is crack sprouting, the second stage is crack development, and the third stage is crack penetration. In the first stage, the cement slurry only fills the existing cracks around the grouting holes, such as cement slurry expansion of 1 MPa grouting pressure. In the second stage, after the cement slurry is filled with the existing cracks, the stress of the grout at the crack tip increases with the increase of time, which promotes the occurrence of micro-cracks at the existing crack tip, and then makes the slurry split rock mass increase the reinforcement range. For example, after 24000 time step of 2 MPa grouting pressure, 22000~30000 time step of 3 MPa grouting pressure and 20000~26000 time step of 4 MPa grouting pressure, cracks are always in the developing stage. In the third stage, cracks are continuously developed and connected with other existing cracks, which further enlarges the range of reinforcement, mainly at the time step of 30,000 and 26000 of 3 MPa and 4 MPa grouting pressure.

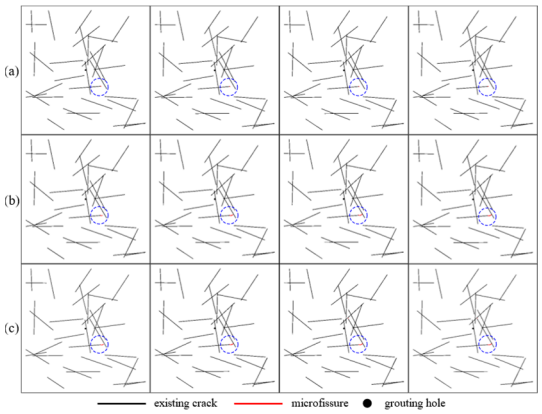

Figure 11: Micro-crack propagation at 26000, 30000, 34000 and 38000 steps under different grouting pressures (a) 2 MPa grouting pressure (b) 3 MPa grouting pressure (c) 4 MPa grouting pressure

4.2 Variation Law of Particle Displacement of Fractured Rock Mass under Different Grouting Pressures

As can be seen from Figure 12 (a), the rock mass is cut by existing cracks, and the rock mass particles will move along the developed part of the cracks under the action of grouting pressure. As shown in Figure 12(b), under the action of four grouting pressures, the maximum displacement of particles reaches 0.078mm, 0.225mm, 0.796mm and 0.980mm respectively. With the extension of grouting time, the maximum displacement of particles reaches stability and no longer increases. Among them, under 3 MPa and 4 MPa grouting pressure, the particle displacements have a sudden increase trend at 30000 and 26000 time step, respectively. Because at this stage, the micro-cracks are connected with the existing cracks, which leads to the sudden increase of particle displacement.

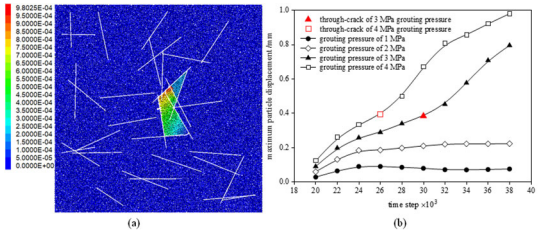

Figure 12: Maximum particle displacement (a) at 38000 time step under 4 MPa grouting pressure (b) at saveral time step under different grouting pressures

4.3 Variation Law of Stress Field of Fractured Rock Mass under Different Grouting Pressures

As shown in Figure 13, under different grouting pressures, the horizontal stress of fractured rock mass continuously radiates outward along the fracture development area. Combined with Figure 8, it can be seen that the maximum horizontal stress is concentrated at the developing part of micro-crack, and it also verifies the stress concentration phenomenon of horizontal stress at the existing crack tip during the grouting process. As can be seen from Figure 14, the horizontal stress tends to be stable with the increase of grouting time step, where under 1 MPa grouting pressure fractured rock mass reaches the maximum value of 8.08 MPa at 26000 time step. The fractured rock mass reaches a maximum of 17.36 MPa at 38000 time step under 2 MPa grouting pressure. Besides under 3 MPa it reaches the maximum horizontal stress of 20.15 MPa at 24000 time step. And the fractured rock mass reached 20.91 MPa at 24000 time step under 4MPa grouting pressure. Under the grouting pressure of 1 and 2 MPa, the horizontal stress increases with the increase of time step, and finally reaches stability. However, 3 MPa and 4 MPa are in the crack penetration stage at 30000 and 26000 time step respectively, which results in the rapid decrease of stress in rock mass. Under the action of 2 MPa grouting pressure, the crack penetration threshold of the third stage is not 20.15 MPa. Therefore, with the increase of grouting pressure, the grout fills the existing cracks around the rock, and the horizontal stress in the fractured rock keeps a high level and constant.

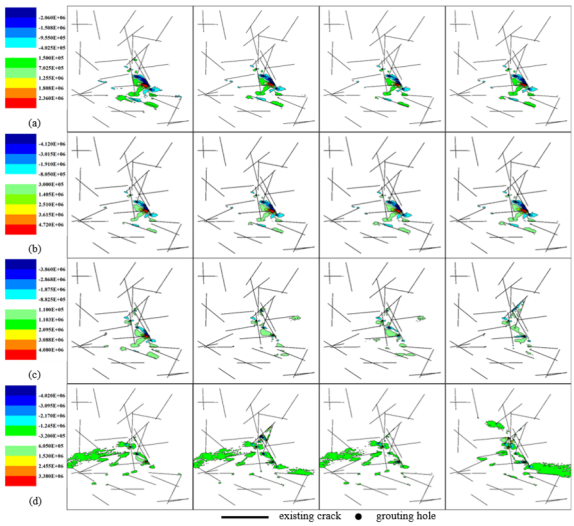

Figure 13: Horizontal stress at 26000, 30000, 34000 and 38000 under different grouting pressures (a) 1 MPa grouting pressure (b) 2 MPa grouting pressure (c) 3 MPa grouting pressure (d) 4 MPa grouting pressure

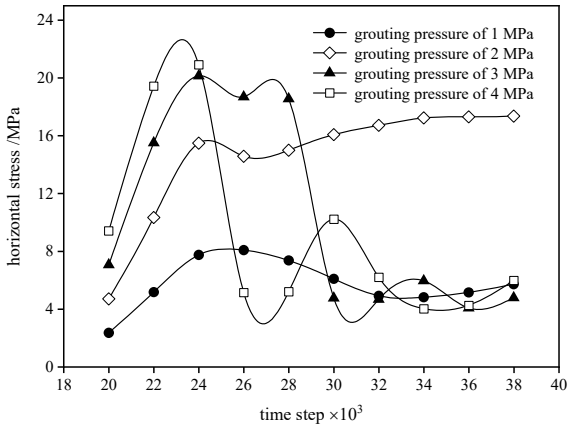

Figure 14: Horizontal stress distribution at each time step under different grouting pressures

5. Conclusion

In this paper, particle discrete element software is used to study the filling and diffusion effects of cement slurry in cracks, particle displacement and stress variation rules under different grouting pressures on limestone fractured rock mass based on random fracture network model. The main conclusions are as follows:

(1) Since the slurry diffusion filling effect of fractured rock body under different grouting pressure is different, based on the different states of slurry diffusion filling, it is divided into 3 stages, which are crack sprouting stage, crack development stage and crack penetration stage.

(2) Under the action of different grouting pressure, with the increase of grouting time, the micro-cracks expand along the tip of existing cracks and have the tendency to extend to the surrounding cracks, and finally form through cracks when the grouting pressure reaches the threshold, so that the existing cracks are connected to each other to achieve the effect of grouting reinforcement.

(3) With the increase of grouting pressure, the maximum particle displacement increases continuously. However, when the fractured rock mass produces through cracks, the maximum particle displacement increases abruptly. However, with the extension of grouting time, the maximum particle displacement eventually reaches a stable state and does not increase.

(4) In the process of grouting, with the increase of grouting time, the horizontal stress of the fractured rock mass finally reaches stability. In the process of grouting, due to the stress concentration of the crack tip, the micro crack expands along the existing crack tip and extends to the surrounding crack. When the stress threshold of the fractured rock mass is exceeded, the through crack is formed, and the stress of the fractured rock mass decreases rapidly after the formation of the through crack. With the increase of grouting time, it finally keeps constant at lower stress level.

Acknowledgements

The work was supported by Natural Science Foundation and Frontier Research Program of Chongqing Science and Technology Commission of China (award number: cstc2013jcyjA30005).

References

1. Y.X. Wang, H. Zhang, H. Lin, et al. Mechanical Behavior and Failure Analysis of Fracture-Filled Gneissic Granite, Theoretical and Applied Fracture Mechanics, vol. 108 (2020), p. 102674.
2. Z.D. Zhu, Z.H. Niu, X.C. Que, et al. Study on Permeability Characteristics of Rocks with Filling Fractures Under Coupled Stress and Seepage Fields, Water, vol. 12 (2020), no. 10, p. 2782.
3. Y.L. Zhao, Q. Liu, C.S. Zhang, et al. Coupled Seepage-Damage Effect in Fractured Rock Masses: Model Development and a Case Study, International Journal of Rock Mechanics and Mining Sciences, vol. 144 (2021), p. 104822.
4. W.Q. Zhang, H.T. Zhou, W.H. Guo: Experimental Study on Seepage Characteristics of Fractured Rock Mass and its Electrical Response, Journal of Hydrologic Engineering, vol. 24 (2019), no. 7, p. 04019017.
5. X.M. Jiang, G.S. Zheng, W.H. Sui, et al. Anisotropic Propagation of Chemical Grouting in Fracture Network with Flowing Water, ACS Omega, vol. 6 (2021), no. 7, p. 4672-4679.
6. X.L. Li, M.M. Hao, Y.H. Zhong, et al. Experimental Study on the Diffusion Characteristics of Polyurethane Grout in a Fracture, Construction & Building Materials, vol. 273 (2021), p. 121711.
7. X.M. Du, C. Liu, C.J. Wang, et al. Diffusion Characteristics and Reinforcement Effect of Cement Slurry on Porous Medium Under Dynamic Water Condition Considering Infiltration, Tunnelling and Underground Space Technology, vol. 130 (2022), p. 104766.
8. W.Q. Ding, C. Duan, Q.Z. Zhang: Experimental and Numerical Study on a Grouting Diffusion Model of a Single Rough Fracture in Rock Mass, Applied Sciences, vol. 10 (2020), no. 20, p. 1-23.
9. D.H. Jiang, X.Z. Cheng, H.J. Luan, et al. Experimental Investigation on the Law of Grout Diffusion in Fractured Porous Rock Mass and its Application, Processes, vol. 6 (2018), no. 10, p. 191.
10. E.M. Zhang, Y.C. Xu, Y. Fei, et al. Influence of the Dominant Fracture and Slurry Viscosity on the Slurry Diffusion Law in Fractured Aquifers, International Journal of Rock Mechanics and Mining Sciences, vol. 141 (2021), p. 104731.
11. W.T. Liu, Y.B. Liu, Y.H. Du, et al. Study on the Development and Distribution Rule of Tensile Shear Fracture Propagation Angle of Fractured Rock Mass Under Seepage Pressure, Geotechnical and Geological Engineering, vol. 37 (2019), no. 5, p. 4151-4161.
12. C. Liu, X.S. Huang, W.P. Yue, et al. Extension of Grouting-Induced Splitting Fractures in Materials Similar to Coal Rocks Containing Prefabricated Fractures, Journal of Geophysics and Engineering, vol. 17 (2020), no. 4, p. 670-685.
13. F. Xiao, Z.Y. Zhao: Influence of Fracture Deformation on Grout Penetrability in Fractured Rock Masses, Tunnelling and Underground Space Technology, vol. 102 (2020), p. 103431.
14. C.W. Zhu, W. Wu, H.W. Ying, et al. Drainage-Induced Ground Response in a Twin-Tunnel System through Analytical Prediction Over the Seepage Field, Underground Space, vol. 7 (2022), no. 3, p. 408-418.
15. Z.G. Zhang, M.D. Mao, Y.T. Pan, et al. Experimental Study for Joint Leakage Process of Tunnel Lining and Particle Flow Numerical Simulation, Engineering Failure Analysis, vol. 138 (2022), p. 106348.
16. K.K. Panthi, B. Nilsen: Uncertainty Analysis for Assessing Leakage through Water Tunnels: A Case from Nepal Himalaya, Rock Mechanics and Rock Engineering, vol. 43 (2010), no. 5, p. 629-639.
17. H. Su: Application of Discrete Element Particle Flow in Hydraulic and Geotechnical Engineering (Science Publications, China 2017), p.129.
18. P.T. Wang, F.H. Ren, W.H. Tan, et al. Model of Roughness Discrete Fractures Network for Uniaxial Compressive Test and its Mechanical Properties, Yan Tu Li Xue, vol. 38 (2017), p. 70-78.
19. X.Q. Wang: Study on Model Reconstruction and Mechanical response Characteristics of jointed coal (Ph.D., China University of Mining and Technology (Beijing), China 2017), p. 25.